VIBGYOR ePress

International Journal of
Metallurgy and Metal Physics

Microstructure and Mechanical Properties of Metal Injection Molding HK30 Stainless Steel Sintered in N_2 and Ar Atmosphere

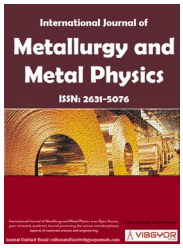

ISSN: 2631-5076

***Yong Yu*[1], *Yimin Li*[1,2*], *Jia Lou*[3], *Hao He*[2], *Youhua Hu*[1] *and Xiang Zhang*[1]**

[1]*State Key Laboratory of Powder Metallurgy, Central South University, China*

[2]*Research Centre for Materials Science and Engineering, Guangxi University of Science and Technology, China*

[3]*School of Materials Science and Engineering, Xiangtan University, China*

Abstract

The effects of different sintering atmospheres (nitrogen and argon) on the densification, microstructure, and mechanical properties of HK30 stainless steel were studied. Compared with those of the samples sintered in Ar, sintered samples in N_2 had a lower density and higher N content. Some of the N atoms dissolved into the austenite matrix, and others were combined with metal atoms to be precipitated along the grain boundaries. Samples sintered in N_2 had a higher hardness than those in Ar. The hardness decreased with the distance from the edge to the center. The highest hardness was 360 $HV_{1.0}$ at the edge, the lowest one was 220 $HV_{1.0}$ at the center. The samples sintered in N_2 had a higher tensile strength than those sintered in Ar at testing temperatures from room temperature to 1000 °C.

Keywords

Metal injection molding, HK30 stainless steel, Sintering atmosphere, Microstructure, Mechanical properties

Introduction

As a heat-resistant austenitic stainless steel, HK30 stainless steel has good oxidation resistance and has high temperature strength up to 600 °C. It is widely used in high temperature environments such as turbocharger vanes. However, stainless steel parts with complex shapes are difficult to manufacture by traditional methods such as casting and machining. Hence, as a near-net-shape method, metal injection molding (MIM) [1-5] is employed to produce stainless steel parts [6-10].

Some researchers have studied the impact of the sintering process on mechanical properties of MIM HK30 alloy. Kearns, et al. [11] studied the effects of powder size and sintering atmosphere on the mechanical properties of MIM HK30. The N_2 atmosphere has a significant effect on the final properties of the products [12]. As a strong austenite stabilizer, nitrogen can effectively save the using of nickel in austenitic stainless steels [13]. With the

***Corresponding author:** *Yimin Li, State Key Laboratory of Powder Metallurgy, Central South University, 410083, Changsha; Research Centre for Materials Science and Engineering, Guangxi University of Science and Technology, 545006, China*

Accepted: May 16, 2019; **Published:** May 18, 2019

ISSN 2631-5076

Citation: Yu Y, Li Y, Lou J, He H, Hu Y, et al. (2019) Microstructure and Mechanical Properties of Metal Injection Molding HK30 Stainless Steel Sintered in N_2 and Ar Atmosphere. Int J Metall Met Phys 4:030

addition of nitrogen, the strength, hardness, wear resistance, and corrosion resistance of austenitic stainless steels are much higher [14-16]. In addition, N-added austenitic stainless steels can solve the "nickel allergy" harm when used for medical materials [17]. However, uniform penetration of nitrogen is difficult to achieve, which leads to uneven performance [18]. Moreover, nitrogen can combine with metal atoms and then be precipitated at grain boundaries, and these precipitates degrade the toughness of the alloy [19]. It is well known that nitrogen can improve the performance of stainless steel at room temperature, but the high temperature properties have not been discussed.

In this study, MIM HK30 was sintered in nitrogen and argon atmospheres. The effects of the sintering atmosphere on the microstructure and mechanical properties were analyzed, including the properties at room temperature and high temperature. The results of this work are of practical significance to guide the actual production of MIM HK30 products.

Experimental Procedures

The gas-atomized HK30 SS powders used in this work were provided by Sandvik Osprey Ltd. The composition, particle size, and particle morphology of the powders can be found in a previous work [20]. The main components of the binder were paraffin wax (PW), stearic acid (SA), polypropylene (PE), and vegetable oil. The binder was mixed with HK30 powder, and the powder loading was 58 vol%. The tensile samples were prepared by injection molding. The dimensions of the tensile sample can be found in a previous work [20]. The green parts were solvent debound at 36 °C in methylene chloride for 6 h, followed by a thermal debinding and presintering at 800 °C for 1 h in argon. Sintering was performed at 1280 °C for 7 h in Ar or N_2 (12 kPa). The dew-points of Ar and N_2 were -60 °C and -26 °C respectively.

The density of the sample was measured by the Archimedes method, and the microstructure was observed with a Polyvar Met metalloscopical microscope. The sample was separated into small pieces to test the hardness. The hardness was tested using a MicroMet-5140 micro-hardness instrument from the edge to center, and the average value of each sample was calculated from 10 data points. The tensile strength and elongation of the material were measured using an Instron universal tester from room temperature to 1000 °C, at a tensile speed of 2.0 mm/min. The N content was tested with a LECO TCH600 oxygen & nitrogen analyzer. The EPMA point analysis and surface scanning analysis of the samples were performed in an electron field emission JXA-8530F electron probe microanalyzer at the acceleration voltage of 15 kV. The diffraction peaks of austenite and nitride were obtained by D/max 2550 X-ray diffraction (XRD) analysis with Cu-Kα radiation.

Results and Discussion

Densification

The sintered densities of samples sintered in nitrogen and argon were 7.48 g/cm^3 and 7.62 g/cm^3, respectively; in other words, under the same conditions, the density in the case of N_2 sintering is lower than in the case of Ar. The N content of the Ar sintered sample was 0.05%, and the N content of the N_2 sintered sample was 0.18%. During the sintering, nitrogen will enter the steel to form nitrides; this hinders the diffusion of iron or chromium and slows down the densification rate [18]. Moreover, the dew point of the N_2 was higher than that of Ar; thus, more H_2O or O_2 is contained in the N_2, resulting in the formation of oxide layer during sintering. Oxide films can also hinder the diffusion and formation of the sintered neck during sintering [21]; therefore, the density in the case of N_2 sintering is lower than in the case of Ar.

Microstructure

Figure 1 shows the microstructures of the samples sintered in Ar and N_2. The sample sintered in Ar shows a homogeneous microstructure, and the grain boundaries are thin and smooth. On the other hand, the sample sintered in N_2 is associated with a large volume of pores. The center region of the sample sintered in N_2 is similar to the sample sintered in Ar. However, there are some needle-like phase precipitated at the edge region, as shown in Figure 2. The region rich in the needle-like phase is about 100 μm in width, and the predicated phase is about 10 μm in length. The length of the precipitates is not uniform.

Figure 3 shows the surface distribution of elemental N in the HK30 alloy. It can be seen that some of the N atoms are dissolved in austenite, and others are accumulated at the grain boundaries. The diffraction peaks of austenite and nitride were obtained by X-ray diffraction (XRD) analysis, as shown in Figure 4. It can be seen that the strip

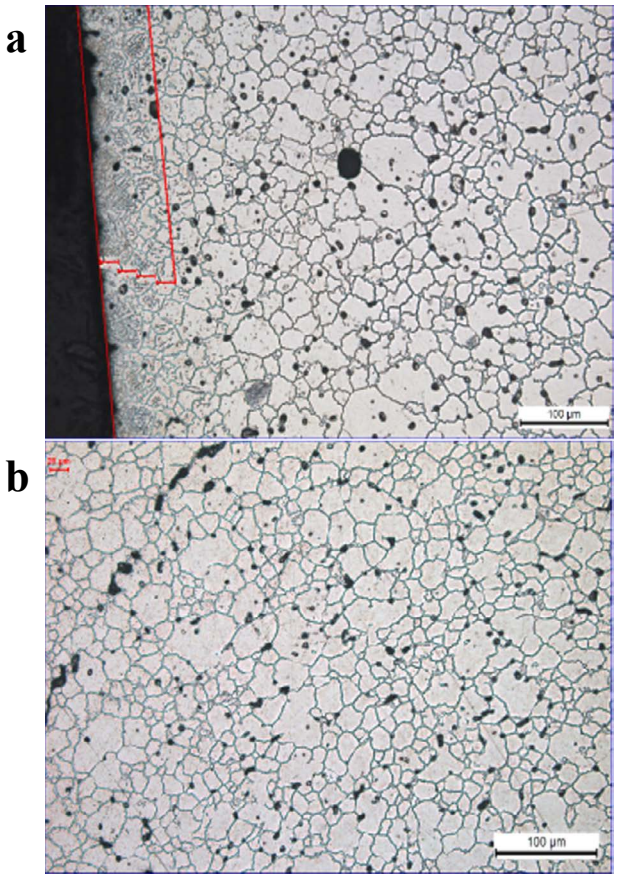

Figure 1: Microstructures of samples sintered under different atmospheres. a) N_2 and b) Ar.

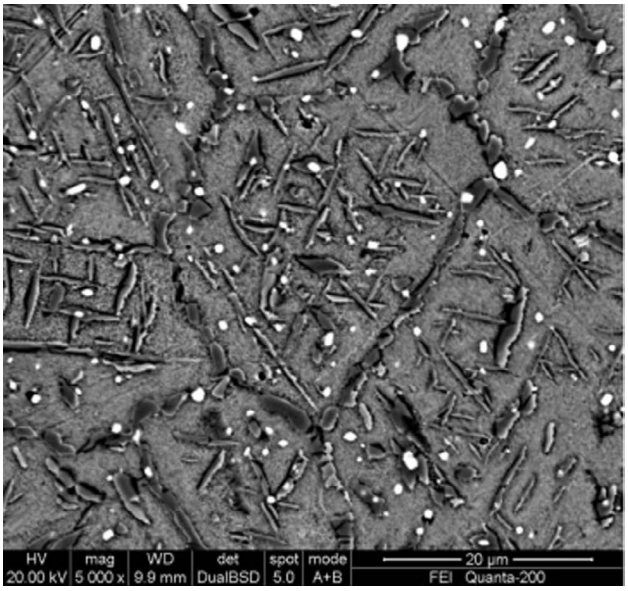

Figure 2: SEM image of edge region of sample sintered in N_2.

should be Cr_2N.

Mechanical properties

Figure 5 shows the distribution of hardness from samples sintered in N_2 and Ar. The hardness of samples sintered in Ar is almost independent of

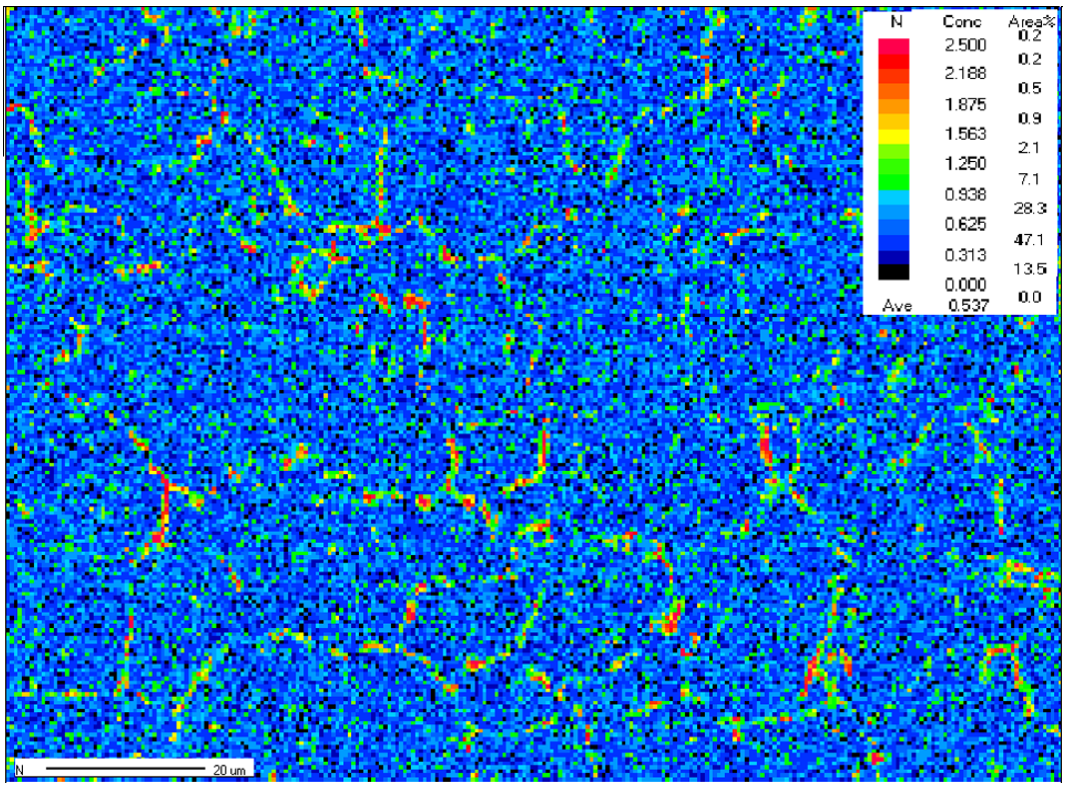

Figure 3: Distribution of elemental nitrogen in the sample sintered in N_2.

Citation: Yu Y, Li Y, Lou J, He H, Hu Y, et al. (2019) Microstructure and Mechanical Properties of Metal Injection Molding HK30 Stainless Steel Sintered in N_2 and Ar Atmosphere. Int J Metall Met Phys 4:030

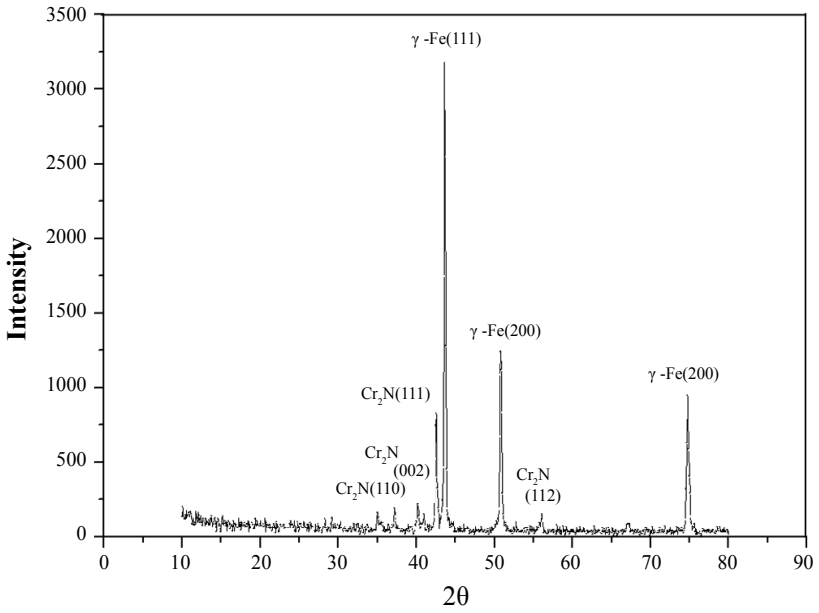

Figure 4: XRD pattern of the sample sintered in N_2.

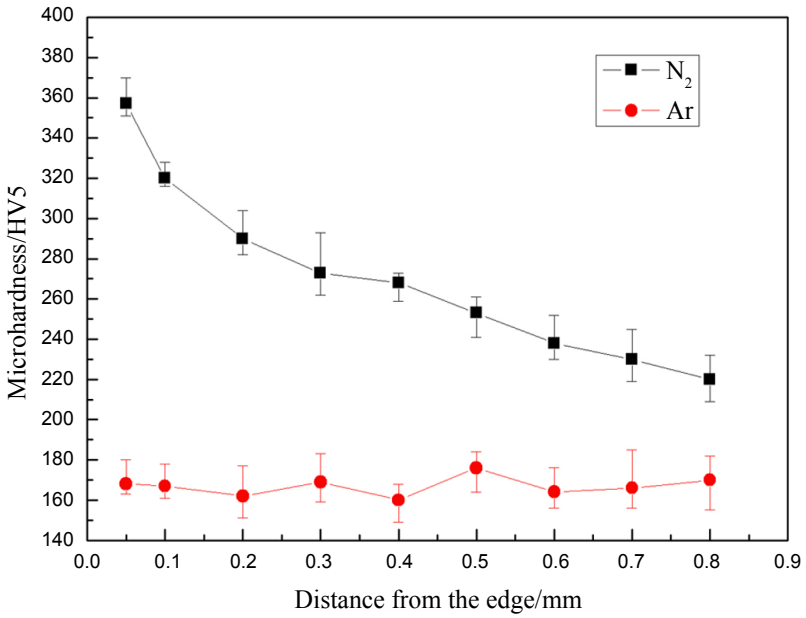

Figure 5: Microhardness distribution of samples sintered in N_2 and Ar.

Table 1: The mechanical properties of samples sintered in N_2 and Ar at room temperature.

Sintering atmosphere	Tensile strength/MPa	Yield strength/MPa	Elongation/%
N_2	650	400	19
Ar	563	276	36

position, and the average hardness is 165 $HV_{1.0}$. On the other hand, the hardness of samples sintered in N_2 is much higher and the hardness decreases with the distance decrease from the edge. The highest hardness is 360 $HV_{1.0}$ at the edge, and the lowest hardness is 220 $HV_{1.0}$ at the center. The infiltration process of nitrogen atoms in austenite is a diffusion process. The nitrogen concentration in different regions of HK30 samples decreases gradually with the increase of the distance from the edge to the

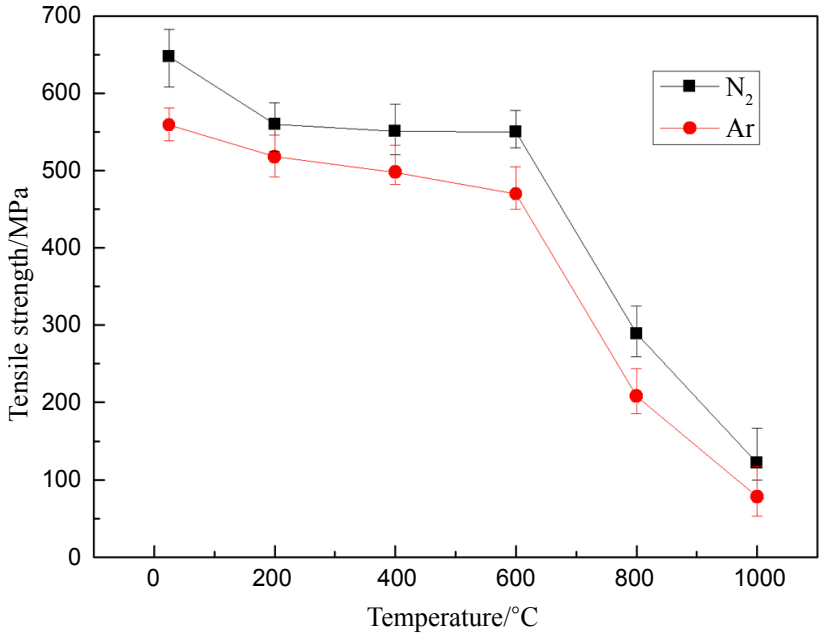

Figure 6: Tensile strength of samples sintered in N_2 and Ar tested at different temperatures.

center, forming a nitrogen concentration gradient that is demonstrated by this hardness curve. The hardness drops more significantly from 0 to 0.2 mm, which is attributed to the existence of the needle-like phase.

At room temperature, the tensile strength and yield strength of the samples sintered in N_2 are significantly higher than those sintered in Ar, as shown in Table 1, however, the elongation of the samples sintered in N_2 is inferior than those sintered in Ar. Figure 6 shows the tensile strength of sintered samples tested at different temperatures. It can be seen that the tensile strength of both samples decreases with the increase of testing temperature, especially in the 600 °C-1000 °C range. The tensile strength of the samples sintered in N_2 is higher than that of the samples sintered in Ar. From the distribution of nitrogen elements before, it can be seen that some of the N atoms are dissolved in austenite, and others are precipitated at the grain boundaries as Cr_2N. The dissolved N atoms stay at the austenitic gap position, which cause lattice distortion and in turn enhance the matrix strength. The precipitated Cr_2N can promote second phase strengthening [22,23]. Thus, the strength of the samples sintered in N_2 is much higher.

Conclusions

1. The samples sintered in N_2 have a lower density and higher N content than samples sintered in Ar. During the sintering, some of the N atoms dissolve into the austenite matrix, while the others combine with chromium to be precipitated at grain boundaries.
2. The samples sintered in N_2 have a higher hardness than the samples sintered in Ar. The hardness of samples sintered in N_2 decreases with the distance from the edge. The highest hardness is 360 $HV_{1.0}$ at the edge. The lowest hardness is 220 $HV_{1.0}$ at the center.
3. The samples sintered in N_2 have a higher tensile strength than the samples sintered in Ar from room temperature to 1000 °C.

Acknowledgement

The authors acknowledge support from the Hunan Provincial Natural Science Foundation (Grant No. 2018JJ3507), the Guangxi Science and Technology Plan Project (Grant No. AD16380019), and the China Postdoctoral Science Foundation (Grant No. 2018M632978).

References

1. J Lou, Y Li, H He, D Li, G Wang, et al. (2017) Interface development and numerical simulation of powder co-injection moulding. Part. I. Experimental results on the flow behaviour and die filling process. Powder Technology 305: 405-410.
2. J Lou, Y Li, H He, D Li, G Wang, et al. (2017) Interface development and numerical simulation of powder

co-injection moulding. Part II. Numerical simulation and experimental verification. Powder Technology 305: 357-363.

3. S Islam, S Samanta, Nagahanumanah, H Roy, AK Lohar, et al. (2018) Rheological behavior of 316L stainless steel feedstock for μ-MIM. Materialstoday: Proceedings 5: 8152-8158.
4. R Machaka, P Ndlangamandla, M Seerane (2018) Capillary rheological studies of 17-4 PH MIM feedstocks prepared using a custom CSIR binder system. Powder Technology 326: 37-43.
5. S Ani, A Muchtar, N Muhamad, JA Ghani (2014) Binder removal via a two-stage debinding process for ceramic injection molding parts. Ceramics International 40: 2819-2824.
6. M Kearns, T Tingskog, A Coleman, K Murray, V Ryabinin, et al. (2014) A study of microstructure and mechanical properties of metal injection moulded HK-30. PM World Congress, Orlando, USA.
7. M Yousefi, M Farghadin, A Farzadi (2015) Investigate the causes of cracks in welded 310 stainless steel used in the flare tip. Engineering Failure Analysis 53: 138-147.
8. M Khan, Q Wang (2013) Investigation of crack initiation and propagation behavior of AISI 310 stainless steel up to very high cycle fatigue. International Journal of Fatigue 54: 38-46.
9. A Bahrami, A Ashrafi, S Rafiaei, MY Mehr (2017) Sigma phase-induced failure of AISI 310 stainless steel radiant tubes. Engineering Failure Analysis 82: 56-63.
10. H Sun, Y Sun, R Zhang, M Wang, R Tang, et al. (2015) Study on hot workability and optimization of process parameters of a modified 310 austenitic stainless steel using processing maps. Materials and Design 67: 165-172.
11. K Martin, P Davies (2007) Review of the MIM industry: Recent trends in powder size and composition. Advances in Powder Metallurgy and Particulate Materials 1: 04.
12. H Zhang, H He, Y Li, X Zhang (2017) Effect of carbon content on microstructure and mechanical properties of metal injection molded HK30 stainless steel. Materials Science and Engineering of Powder Metallurgy 22: 739-746.
13. FC Hull (1973) Delta ferrite and martensite formation in stainless steels. Welding Journal 52: 193-195.
14. H He, Y Li, D Li (2011) Effect of sintering temperature and atmosphere on corrosion behavior of MIM 316L stainless steel. Advanced Materials Research 239-242: 132-136.
15. JHG (1951) Monypenny. Stainless Iron and Steel. Chapman & Hall Ltd, London, 125-144.
16. S Kubota, Y Xia, Y Tomota (1998) Work-hardening behavior and evolution of dislocation microstructures in high-nitrogen bearing austenitic steels. ISIJ Intnl 38: 474-476.
17. L Reclaru, R Ziegenhagen, PY Eschler, A Blatter, J Lemaitre (2006) Comparative corrosion study of "Ni-free" austenitic stainless steels in view of medical applications. Acta Biomaterialia 2: 433-444.
18. C Dawei, W Jinglong (2013) Research on powder metallurgy high nitrogen stainless steels. Advanced Materials Research 690-693: 172-175.
19. Sung Joon Kim, Tae Ho Lee, Chang-Seok Oh (2009) Effect of nitrogen on the deformation behaviour of high-nitrogen austenitic stainless steels. Steel Research International 80: 467-472.
20. Hu Y, Li Y, Lou J, He H, Zhang X (2018) Effects of sintering temperature and holding time on densifcaton and mechanical properties of MIM HK30 stainless steel. Int J Metall Met Phys 3: 022.
21. H He, J Lou, Y Li, H Zhang, Y Shuai, et al. (2018) Effects of oxygen contents on sintering mechanism and sintering-neck growth behaviour of Fe-Cr powder. Powder Technology 329: 12-18.
22. L Jun, Y Yixun, R Yibin, D Jiahui, Y Ke (2018) Effect of cold deformation on corrosion fatigue behavior of nickel-free high nitrogen austenitic stainless steel for coronary stent application. Journal of Materials Science & Technology 34: 86-91.
23. S Feng, L Xiaowu, Q Yang, L Chunming (2013) Effects of cold deformation and aging process on precipitation behavior and mechanical properties of Fe-18Cr-18Mn-0.63N high-nitrogen austenitic stainless steel. Steel Research International 84: 1034-1039.

ISSN 2631-5076